Tailoring higher-order van Hove singularities in non-Hermitian interface systems via Floquet engineering

Ayan Banerjee [1,*,†] Debashree Chowdhury [2,*,‡] and Awadhesh Narayan [1,§]
[1] *Solid State and Structural Chemistry Unit, Indian Institute of Science, Bangalore 560012, India*
[2] *Centre of Nanotechnology, Indian Institute of Technology Roorkee, Roorkee 247667, Uttarakhand*

(Received 6 October 2023; accepted 28 November 2023; published 14 December 2023)

We propose a non-Hermitian (NH) interface system formed between two NH nodal line semimetals driven by optical fields as a platform for generation and tailoring of higher-order van Hove singularities (VHS). Through an analytical analysis of the density of states (DOS), we find VHS with logarithmic divergences in the Hermitian limit. Upon introducing NH terms, four exceptional rings on two sides of the Fermi line are formed. By tuning the NH parameters and the light amplitude, we find a situation when one exceptional ring crosses the Fermi line, where a saddle point appears and results in a paired VHS around the origin. In contrast, when an exceptional contour resides at the Fermi energy, the saddle points critically get destroyed and we obtain a single peak in the DOS, with power-law divergences. These higher-order divergences that appear in an NH system have a different origin than that of the higher-order VHS in Hermitian systems, where no saddle point merging is noted. Our results suggest NH interfaces to be promising avenues for exploring higher-order VHS.

DOI: 10.1103/PhysRevB.108.235148

I. INTRODUCTION

The advent of topological phases has become an intriguing aspect of condensed matter physics [1–3]. Starting with the unique features of two- and three-dimensional topological insulators [4–6], the new focus now are the semimetallic phases that appear in different systems. What makes these semimetal phases alluring are the isolated band-crossing points or lines, which may result from band inversion [7,8]. These unique band crossings are related to the monopoles of Berry phases. So far, three different kinds of semimetals are among the most explored, namely Dirac semimetals [9–12], Weyl semimetals [8,13], and nodal line semimetals [14–16]. In the case of Dirac semimetals fourfold degenerate Dirac points appear in the system, which are protected by crystalline symmetries. In Weyl semimetals, the band crossing points, coined as Weyl points, are doubly degenerate and have definite chiralities [17,18]. Furthermore, the topological nodal line semimetals form degeneracy lines in lieu of discrete points in the momentum space [9,15].

On the other hand, topological NH systems are at the forefront of research for condensed matter, optics, and photonics communities [19–32]. The distinctive feature of NH systems is the existence of certain degenerate points where both the eigenenergies, as well as eigenfunctions, of the system coalesce. These degenerate points are known as exceptional points (EP) [33]. These EPs endow unique features in NH topological systems [34–36]. Moreover, in NH systems, enhanced tunability can be achieved by illuminating the system following the well-established principles of Floquet engineering [37,38]. Hermitian topological systems show tunable Fermi surface topology in the presence of time-periodic fields [39–46]. In NH topological systems, however, the understanding of the topology caused due to the combined action of non-Hermiticity and driving is a topic of recent thrust [37]. For instance, circular driving generates new exceptional contours and can cause topological charge division [47].

It is well known that a saddle point in the band structure could cause divergences in the DOS, which is coined as the VHS [48]. This logarithmic divergence in DOS, which, when lying at the Fermi energy, leads to intriguing physics. The VHS spawns effects such as superconductivity, charge, and spin density waves. Interestingly, VHS has intriguing effects on topological systems [49]. Recently, it has been found that deviations from the usual logarithmic singularity may be engineered, resulting in higher-order singularities with a power-law divergence [50,51]. These divergences are the crucial ingredients in understanding the ordering instabilities in systems such as stacked bilayer graphene, twisted bilayer transition-metal dichalcogenides, or even high Tc superconductors and heavy fermions materials [52–56]. In a recent work, it was shown that high-frequency light can induce a logarithmic-type VHS in an interface Hermitian system [57], in the presence of asymmetric light intensities. This raises the question of the nature of the DOS and VHS in non-Hermitian interface systems. The goal of this paper is twofold. First, we would like to highlight the fact that the enhanced VHS (higher order) is a crucial aspect of having various interesting physics in NH interface systems. Recently, there have been several examples which highlight the role of higher order VHS in giving rise to interesting physics [58]. This has motivated us to study higher-order VHS in systems with non-Hermitian

[*] These authors contributed equally to this work.
[†] ayanbanerjee@iisc.ac.in
[‡] debashreephys@gmail.com
[§] awadhesh@iisc.ac.in

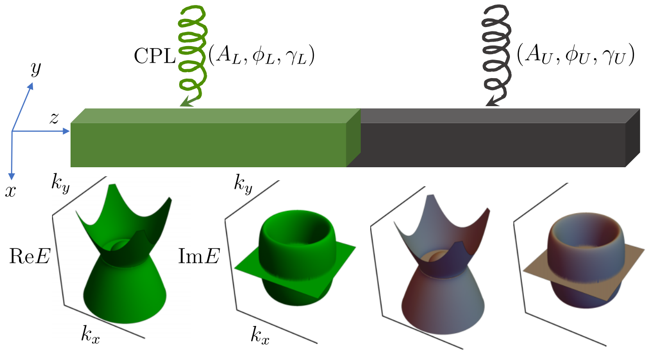

FIG. 1. Conceptual illustration of the NH interface system. The schematic representation illustrates the arrangement of the non-Hermiticity-induced nodal line semimetals divided into two regions—lower ($z < 0$) and upper ($z > 0$) half-spaces. These regions are subjected to high-frequency monochromatic circularly polarized light (CPL) irradiation with distinct intensities, polarizations, and non-Hermiticity coefficients denoted as (A_L, ϕ_L, γ_L) for the lower half-space and (A_U, ϕ_U, γ_U) for the upper half-space. In the presence of non-Hermiticity, the nodal ring splits into two exceptional rings. Driving allows the tuning of exceptional physics.

loss or gain. Another important goal of our study is to propose mechanisms to tune these VHS points with controllable parameters, such as light amplitude and loss/gain terms. This tuning provides a tool to controllably switch between normal VHS and higher-order VHS under different conditions.

The system we propose contains two nodal line semimetals, with different gain/loss terms, and the two halves are differently illuminated with two opposite circular polarized monochromatic light beams. Figure 1 shows a schematic of our proposal. In this scenario, the energy spectra and the DOS show unique features that are absent in the Hermitian limit. The band structure of the system is rich enough, resulting in regions where the Fermi line falls within or on one of the exceptional contours, which shows unique Fermi surface topology. When non-Hermiticity is introduced on both sides ($\gamma_L, \gamma_U > 0$), the two nodal rings of the Hermitian limit are broken into four exceptional rings [located on the two sides of the Fermi line $\mathrm{Re}(E) = 0$]. Consequently, one obtains eight EPs along the k_x axis. When one of such exceptional rings crosses the Fermi line, a saddle point at a high symmetry point ($k_x = 0, k_y = 0$) appears, resulting in a paired VHS around the origin. If an exceptional contour resides on the Fermi energy, the saddle points critically get destroyed along the k_x axis, and a single peak in the DOS is obtained, which at a higher resolution splits into two peaks with the emergence of higher order ($E^{1/3}$ and $E^{1/2}$) power law divergences. In NH systems, these higher-order singularities appear not because of the saddle points but rather due to saddle point coalescing [59].

II. THE MODEL HAMILTONIAN

The Hamiltonian of the nodal ring semimetal with the NH term is written as [60]

$$H(k) = \left[m - B\left(k_x^2 + k_y^2 + k_z^2\right)\right]\sigma_x + i\gamma\sigma_y + v_z k_z \sigma_z, \quad (1)$$

where σ_i $(i = x, y, z)$ are Pauli matrices that represent the two orbitals and v_z is the Fermi velocity in the direction of k_z. Additionally, m and B are parameters characterized by energy units and inverse energy units, respectively. In the Hermitian limit, when $mB > 0$, the conduction and valence bands intersect, forming a nodal ring in the $k_z = 0$ plane at $k_x^2 + k_y^2 = m/B$ [45,46]. Conversely, for $mB < 0$, the system exists within the trivial insulator phase, featuring an energy gap. To simplify matters, and without loss of generality, it is assumed from here on that m, B, and v_z are all positive unless explicitly stated otherwise. This Hermitian nodal ring remains protected by the joint symmetries of inversion (P) and time reversal (T), represented as PT [45]. In the presence of an NH term $i\gamma$ that accounts for the dissipative coupling manifesting "imaginary Zeeman fields" [29,61], the original nodal ring breaks into two exceptional rings along $k_z = 0$. The NH term inherently breaks the PT symmetry but respects the chiral symmetry. As γ increases, the inner exceptional ring progressively contracts and eventually disappears beyond a critical point at $\gamma = m$, condensing into a point.

For $k_z = 0$ we have $(k_x^2 + k_y^2) = \frac{m\pm\gamma}{B}$, which gives the nodal ring in the k_x-k_y plane. Next, we drive the system with light polarized along the y-z plane and the vector potential associated with it is $\boldsymbol{A}(t) = A(0, \cos(\omega t), \sin(\omega t + \phi))$. Here A and ω are the amplitude and frequency of the incident light. Also, $\phi = 0$ $(\phi = \pi)$ corresponds to the right (left) circular polarization. Application of periodically time-driven light allows us to use the Floquet formalism, which in the high-frequency limit provides the effective Hamiltonian [37,39,40,62–71],

$$H_F(k) = \left[\tilde{m} - B\left(k_x^2 + k_y^2\right)\right]\sigma_x + v_z k_z \sigma_z + \left(\lambda k_y + i\gamma\right)\sigma_y, \quad (2)$$

where $\tilde{m} = m - Be^2A^2$ and $\lambda = -\frac{2e^2BvA^2\cos\phi}{\omega}$. The corresponding energy eigenvalues are

$$E_\pm(k) = \pm\sqrt{\left[\tilde{m} - B\left(k_x^2 + k_y^2\right)\right]^2 + v_z^2k_z^2 + (\lambda k_y + i\gamma)^2}. \quad (3)$$

The exceptional degeneracies delineating a pair of EPs for $\lambda \neq 0$ and $k_y = k_z = 0$ are found at

$$k_x = \pm\sqrt{\frac{\tilde{m} \pm \gamma}{B}}. \quad (4)$$

The exceptional degeneracies, which appear for $\mathrm{Re}(E) = 0$ and $\mathrm{Im}(E) = 0$, are accompanied by a Fermi arc along the k_x axis protected by nontrivial Z topology for a real line gap [72]. We note that the chirality of the exceptional rings depends simply on the handedness, $\cos\phi$, of the incident laser beam. Moreover, the shape and position of the exceptional rings are tunable by changing the direction and amplitude of the incident laser beams. The topological characterization, as well as Hall signatures in this light-driven system, have been recently studied in the literature [73,74]. Here we examine the NH interface system and explore the exceptional VHS arising from Lifshitz transitions with striking changes in the Fermi surface topology, considering the interplay of laser driving and non-Hermiticity.

III. INTERFACE BETWEEN TWO NH NODAL LINE SEMIMETALS AND DENSITY OF STATES

We consider an interface of two nodal ring semimetals with different light intensities and NH parameters on the two sides (see Fig. 1). The effective Floquet Hamiltonian for each side is written as

$$H_j(k) = [\tilde{m}_j - Bk^2]\sigma_x + (\lambda_j k_y + i\gamma_j)\sigma_y + v_z k_z \sigma_z, \tag{5}$$

where $\tilde{m} = m - Be^2A_j^2$, $\lambda_j = -\frac{2e^2BvA_j^2\cos\phi_j}{\omega}$ with $j \in U, L$, and $k^2 = k_x^2 + k_y^2 + k_z^2$. The interface is considered along the z direction and is located at $z = 0$. This system is subjected to the influence of two light beams with opposite circular polarizations. When we consider the high-frequency scenario, we employ an effective Floquet Hamiltonian for each of these regions [64]. Specifically, we label the right ($z > 0$) and left ($z < 0$) half-spaces as H_U and H_L, respectively. In Fig. 1, we have presented a schematic of our setup. Here, the subscripts L and U signify the left and right half-spaces, respectively. However, the sign of the product $\lambda_U\lambda_L$ is negative due to the contrasting circular polarizations of the two light beams. Notably, the assumption we make about the interface between these regions having an abrupt sharpness does not diminish the validity of our results, as the emergent topological interface modes are resilient against perturbations at the interface.

The stationary Schrödinger equation, linked to each half-space, is given by

$$\mathcal{H}_j(\boldsymbol{k}_\perp, k_z \to -i\partial_z)\psi_j(\boldsymbol{r}) = E(\boldsymbol{k}_\perp)\psi_j(\boldsymbol{r}), \tag{6}$$

where $\boldsymbol{k}_\perp = (k_x, k_y)$ and $E(\boldsymbol{k}_\perp)$ is the eigenenergy. We consider the following ansatz wave function:

$$\psi_j(r) = e^{ik_x x}e^{ik_y y}\begin{pmatrix}\psi_1^j & \psi_2^j\end{pmatrix}e^{\mu_j z}. \tag{7}$$

The real part of $\mu_j z$ [$\mathrm{Re}(\mu_j z) < 0$] dictates the spatial localization in proximity to the plane $z = 0$. Substituting Eq. (7) into Eq. (6) yields the secular equation governing the eigenstates

$$\det[H(\boldsymbol{k}_\perp, \partial_z \to \mu_j) - E\mathcal{I}] = 0, \tag{8}$$

where $\mu_j = \frac{1}{v_z}\sqrt{[\tilde{m}_j - Bk^2]^2 + (\lambda k_y + i\gamma)^2 - E^2}$. The interface energy for each half-space is written as [57]

$$E(\boldsymbol{k}_\perp) = \frac{(-i\alpha_L\gamma_U + i\alpha_U\gamma_L + k_y\alpha_U\lambda_L - k_y\alpha_L\lambda_U)}{\sqrt{(\alpha_L - \alpha_U)^2 - (\gamma_U - \gamma_L + ik_y(\lambda_L - \lambda_U)^2)}}, \tag{9}$$

where $\alpha_j = \tilde{m}_j - Bk^2$.

For each perpendicular momentum component $\boldsymbol{k}_\perp = (k_x, k_y)$, the quantity $E(\boldsymbol{k}_\perp)$ is the eigenenergy associated with an interface state. This interface energy is defined when both $\mathrm{Re}[\mu_L]$ and $\mathrm{Re}[\mu_R]$ are nonzero. Conversely, if either $\mathrm{Re}[\mu_L]$ or $\mathrm{Re}[\mu_R]$ is zero, the obtained solution characterizes a delocalized mode across the left or right half-space corresponding to a bulk state. Consequently, the condition $Re[\mu_L\mu_R] = 0$ serves as a defining criterion for establishing the boundaries within the two-dimensional momentum space of interface states. The topological attributes of the interface states are contingent upon the spatial arrangement in the two-dimensional momentum space (k_xk_y) of the surface projections of EPs from the upper and lower exceptional nodal ring semimetals (ENRS). In the present case, this arrangement is dictated by the varying light intensities experienced by the two half-spaces of the ENRS. Precisely, for each half-space, the manipulation of light intensity λ_j, as facilitated by Eq. (3), results in the ability to either bring the EPs closer to or move them further away from the origin of momenta. The bulk Fermi line of this interface is defined as $\mathrm{Re}[E(k_\perp)] = 0$ (the red dotted line in Fig. 2). Figure 2 shows the density plots depicting the energy dispersion characteristics of interface states as a function of $k_\perp$. In the Hermitian limit ($\gamma_j = 0$), in the presence of laser driving ($A_U = 1.25; A_L = 1.95$), the interface states are demarcated by the nodal lines, which are the solutions of $\mu_L = \mu_R = 0$. Notably, along the nodal lines, the interface band coalesces with the bulk conduction and valence bands. Next, switching on the non-Hermiticity enables the splitting of nodal rings to exceptional rings endowing Lifshitz transitions. Consequently, the interface states become bounded by these exceptional rings. Intriguingly, by manipulating the interplay between light intensity and non-Hermiticity, the exceptional rings undergo movement in the momentum space and traverse the Fermi line (indicated by the red dotted line). The analytical conditions for the three qualitatively different non-Hermitian phases corresponding to Fig. 2 are as follows:

(i)

$$\sqrt{\frac{\tilde{m}_L \pm \gamma L}{B}} < \frac{\sqrt{A_U^2\big(-A_L^2B + m\big)\cos(\phi_L) + A_L^2\big(A_U^2B - m\big)\cos(\phi_U)}}{\sqrt{B\big(A_U^2\cos(\phi_L) - A_L^2\cos(\phi_U)\big)}} < \sqrt{\frac{\tilde{m}_U \pm \gamma_U}{B}}, \tag{10}$$

(ii)

$$\sqrt{\frac{\tilde{m}_U - \gamma_U}{B}} < \sqrt{\frac{\tilde{m}_L \pm \gamma_L}{B}} = \frac{\sqrt{A_U^2\big(-A_L^2B + m\big)\cos(\phi_L) + A_L^2\big(A_U^2B - m\big)\cos(\phi_U)}}{\sqrt{B\big(A_U^2\cos(\phi_L) - A_L^2\cos(\phi_U)\big)}} < \sqrt{\frac{\tilde{m}_U + \gamma_U}{B}}, \tag{11}$$

(iii)

$$\sqrt{\frac{\tilde{m}_U - \gamma_U}{B}} < \frac{\sqrt{A_U^2\big(-A_L^2B + m\big)\cos(\phi_L) + A_L^2\big(A_U^2B - m\big)\cos(\phi_U)}}{\sqrt{B\big(A_U^2\cos(\phi_L) - A_L^2\cos(\phi_U)\big)}} < \sqrt{\frac{\tilde{m}_U + \gamma_U}{B}} < \sqrt{\frac{\tilde{m}_L \pm \gamma_L}{B}}. \tag{12}$$

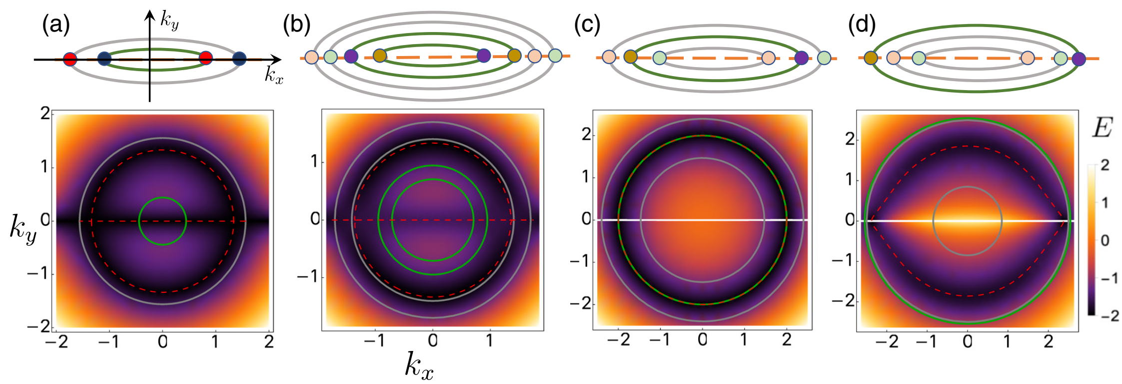

FIG. 2. Illustration of the nodal exceptional rings delineating the Fermi surface spectral topology and energy dispersion of the interface states. The upper panel shows the (a) nodal ring semimetals in the Hermitian limit ($\gamma_U, \gamma_L = 0$), (b)–(d) exceptional rings (shown in gray and green) for the interface system as a function of light intensity. The two nodal rings arising from the interface system under NH perturbation split into four exceptional rings. Consequently, the four Weyl points with opposite chiralities (red and blue dots) along the k_x split into eight EPs. These four exceptional rings consisting of eight EPs move along the k_x axis and can annihilate each other as a function of non-Hermiticity and driving amplitude. The lower panel depicts the density plots of the interface states. The dotted red lines represent the Fermi line $\mathrm{Re}E(k_\perp) = 0$, and we set $v_z = 1$, $\omega = 10$, $B = 0.5$, $m = 2$, $\phi_U = \pi$, and $\phi_L = \pi$. (a) The interface states are bounded by nodal rings residing on the two sides of the Fermi line. The nodal lines define the coalescing of the interface band into a conduction (valence) bulk band for $A_U = 1.25$ and $A_L = 1.95$. (b) The nodal lines split into four exceptional rings (on the two sides of the Fermi line), which delimit the interface states for $(A_U, \gamma_U) = (1.25, 0.23)$ and $(A_L, \gamma_L) = (1.95, 0.35)$. (c) The critical case with six EPs where the green exceptional ring merges on the Fermi line and the gray ring crosses the Fermi line for $(A_U, \gamma_U) = (0.2, 0.9)$ and $(A_L, \gamma_L) = (0.0, 0.0)$. (d) The green ring traverses the Fermi line, and two gray rings are located on the two sides of the Fermi line for $(A_U, \gamma_U) = (0.72, 1.38)$ and $(A_L, \gamma_L) = (1.18, 1.94)$.

These three conditions correspond to Figs. 2(b), 2(c), and 2(d), respectively. These, in turn, lead to noteworthy implications in the DOS, which we delve into next. Using the interface energy, the spectral function can be obtained as

$$\mathcal{A}(\omega) = -\frac{1}{\pi}\mathrm{Im}[\omega + i\eta - E(\boldsymbol{k}_\perp)]^{-1}. \tag{13}$$

The DOS can then be obtained as $\rho(\omega) = \frac{1}{2\pi}\mathcal{A}(\omega)$. We note that, in NH systems, employing a biorthogonal basis composed of both right and left eigenvectors [75], one can construct the NH adaptation of Lehmann's representation of the Green's function [76].

In Ref. [57], the authors have discussed the DOS for two situations. For a symmetric interface with equal light amplitude, the DOS shows a Θ function behavior. However, for unequal light amplitudes applied in the two regions of the nodal line semimetals, a VHS is found to appear in the DOS at the Fermi energy. The VHS in the DOS manifests from the existence of saddle points in the energy dispersion of systems. In two-dimensional Hermitian systems characterized by an energy dispersion $E(k_x, k_y)$, a VHS featuring a logarithmically diverging DOS arises at a saddle point $\mathbf{k}_s$, which is governed by $\nabla_{\mathbf{k}}E = 0$ and $\det D < 0$, where $D_{ij} = \frac{1}{2}\partial_i\partial_j E$ is the Hessian matrix of E at $\mathbf{k}_s$. For instance, consider a Taylor expanded energy dispersion around a saddle point $\mathbf{k}_s$, as $E - E_\xi = -ak_x^2 + bk_y^2$, where E_ξ is the VHS energy. The saddle point criteria are satisfied with the condition $ab < 0$, where the two coefficients $-a$ and b are the eigenvalues of the Hessian matrix D.

We next analyze the saddle point physics and VHS in our NH interface system, considering the interplay of exceptional topology and Fermi surface crossing. We inspect the qualitatively different regimes upon tuning of light intensity and non-Hermiticity coefficient, which enable a topological transition of saddle points. First, we consider the Hermitian case ($\gamma_U = \gamma_L = 0$). We obtain two Weyl rings, consisting of four Weyl points along k_x (red and blue points designate the positive and negative chirality; see Fig. 2). Since the intricate structure of the VHS around this transition point is solely characterized by local energy dispersion near $\mathbf{k}_s$, we expand $E(\mathbf{k})$ near k_s to higher orders, $E - E_\xi = ak_y + bk_y^3 + (dk_y + ek_y^3)k_x^2$. The behavior of the VHS depends crucially on the sign of the coefficients a, b, c, d, and e. For $a/d < 0$, two saddle points appear along the $k_y = 0$ line at momenta $(\pm\frac{i\sqrt{a}}{\sqrt{d}}, 0)$ with the condition $4ad < 0$ resulting in VHS at $E_\xi = 0$ [see Fig. 3(a)].

Next, we move on to different NH cases presented in Fig. 2. Importantly, we focus on the real part of the expanded dispersion near the saddle points, considering the fact that the imaginary parts add broadening to the spectrum. We expand E near k_s to higher orders, $E - E_\xi = \frac{1}{\sqrt{\Theta}}(\alpha_i + \beta k_y + \delta_i k_y^2 + \Gamma k_y^3 + (\zeta_i + \eta k_y + \epsilon_i k_y^2)k_x^2)$. The subscript "$i$" denotes the purely imaginary coefficients. We switch on the non-Hermiticity ($\gamma_L, \gamma_U > 0$) to obtain four exceptional rings (located on the two sides of the Fermi line $\mathrm{Re}[E] = 0$). Consequently, four Weyl points are split into eight EPs along the k_x axis. Interestingly, in this case, the saddle points positions are renormalized on the $k_y = 0$ line with $(\pm\sqrt{-\beta/\eta}, 0)$. They satisfy the criterion $4\beta\eta < 0$, manifesting a VHS at $E_\xi = 0$ with a broadening [see Fig. 3(b)].

We next discuss the critical case of three exceptional rings when two gray rings reside on both sides of the Fermi line, and the green ring coalesces on the Fermi line. In this situation, the saddle points critically get destroyed along the k_x axis.

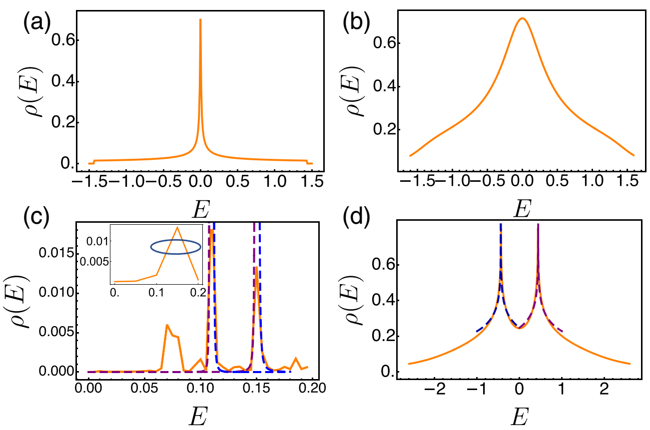

FIG. 3. Density of interface states and VHS physics. (a) The divergence in the DOS manifests in a VHS for the Hermitian case. (b) Switching on the non-Hermiticity leads to broadening in the DOS as long as the green and gray rings lie on the two sides of the Fermi line. (c) The critical case corresponds to a single peak in the DOS, which gives rise to nth root singularities with $n = 2$ and 3 describing higher order VHS. (d) DOS for paired VHS is symmetric about the origin. The dotted blue lines in (c) and (d) designate the power law fitting with $E^{1/2}$ ($E^{1/3}$) and $\log(1/|E|)$ logarithm scaling, respectively.

Consequently, we obtain a single peak in the DOS, which at a higher resolution [50,77] eventually splits into two peaks with the emergence of higher order ($E^{1/3}$ and $E^{1/2}$) power law divergences [see Fig. 3(c)]. Finally, we consider the case where an exceptional ring consisting of two EPs of opposite chirality annihilates with the tuning of non-Hermiticity and light intensity. In this case, one gray ring crosses the Fermi line. Consequently, we obtain a saddle point at the high symmetry point (0,0) with the condition $4\delta_i\zeta_i < 0$, resulting in a pair of VHS symmetric around the origin [see Fig. 3(d)]. It is interesting to add here that by tuning the amplitude of the light and NH parameter, one can have control over the nature of the DOS. It can, in some cases, show normal VHS, whereas, at some points of the spectra, higher-order VHS appears. This higher-order VHS has unique effects on the transport properties of different systems. In a recent work, the authors have shown the role of the higher-order VHS in the arena of thermoelectric transport [58]. It was shown that a type-II nodal-line semimetal, which possesses two VHS near the energy of the nodal line, leads to an increased Seebeck coefficient (S) that eventually provides a large power factor ($S^2\sigma$). It is important to point out here that the electrical conductivity (σ) in this system is also high because of the linear band at the nodal line. As a result, the increased power factor provides a higher value of the figure of merit of these systems. These (and other) types of proposals are also valid in our time-driven interface systems. Apart from thermoelectricity, the enhanced DOS at VHS in time-modulated systems holds promise for exotic applications in the realm of light-matter interaction in quantum optics and condensed matter physics [78,79]. The tailored modulation of VHS in polariton systems opens avenues for advanced quantum information processing and computation, leveraging the enhanced DOS to achieve controlled entanglement and quantum state manipulation [80]. Furthermore, the enhanced DOS at VHS offers a platform for the exploration of exotic quantum phases, potentially leading to the realization of unconventional topological states of matter [81–83]. In the arena of NH topological physics, the enhanced value of DOS at the VHS can provide a controlled manipulation of exceptional surfaces that can be harnessed to create ultrasensitive sensors, enabling high-precision detection in various applications, including quantum sensing and imaging [84]. The enhanced LDOS at VHS emerges as a key principle in these applications, with potential devices at the intersection of quantum optics and condensed matter physics [85]. We hope that our work will initiate some understanding of such links between enhanced DOS and time-driven systems in the NH domain.

IV. DISCUSSION AND CONCLUSION

In conclusion, we have proposed an interface system of two NH nodal line semimetals, driven by light which enables control over higher-order VHS physics. In the Hermitian limit, the DOS shows VHS with logarithmic divergence. However, once non-Hermiticity is switched on, the two nodal rings produce four exceptional rings on two sides of the Fermi line. By tuning the light amplitude and non-Hermiticity, the occurrence of VHS is tuned with the motion and merging of the exceptional rings. We note here that both the tunable parameters, i.e., the light amplitude and the NH parameter, are important for the unique behavior of the VHS in our analysis. The paired VHS, as well as higher-order VHS with $E^{1/3}$ and $E^{1/2}$ power-law divergences, appear in the interface system depending on the values of the driving and NH parameters. Overall, our results suggest NH interfaces to be promising avenues for exploring higher-order VHS and their accompanying physics.

We succinctly outline potential experimental techniques to materialize these exceptional nodal structures [86]. Reference [87] provides a procedural guide for attaining exceptional rings in photonic crystals. A promising avenue for experimentally realizing our proposal involves illuminating a junction between a topological insulator and a ferromagnet, which has been recently identified as a potential platform for realizing NH gapless phases by Bergholtz and Budich [88]. Consequently, illuminating such material junctions emerges as a readily adjustable platform for the observation and manipulation of light-induced NH topological phases [88]. On the other hand, topoelectrical circuits offer a straightforward and effective means to fine-tune these exceptional structures [89–91]. In the realm of topoelectrical circuits, the experimental validation of nodal band structures becomes feasible at a specific resonance frequency, facilitated by a sine wave generator. This involves tracing complex admittance spectra, where distinct changes, reflecting the presence of exceptional rings and alterations in the Fermi surface, can be observed. The flexibility to repeatedly switch circuit parameters on/off at will allows for the realization of periodic driving. An alternative avenue to realize our proposal lies in optically shaken cold atom systems, introducing loss through selective depopulation of cold atoms [92,93]. Achieving the required potential for the exceptional nodal structure involves tuning time-dependent oscillations via controlled interfering laser beams. Finally, the distinctive DOS delineating VHS in these “exceptional heterostructures” can be directly observed through momentum-resolved spectroscopy and angle-resolved photoemission spectral functions [94]. Given the recent strides in experimental capabilities, we are hopeful that our predictions may be accessible in state-of-the-art platforms, particularly in the realm of optical computing and convolution processing [95].

ACKNOWLEDGMENTS

A.B. is supported by the Prime Minister's Research Fellowship (PMRF). D.C. acknowledges financial support from DST (Project No. SR/WOS-A/PM-52/2019). A.N. acknowledges support from a startup grant (SG/MHRD-19-0001) of the Indian Institute of Science.

[1] M. Z. Hasan and C. L. Kane, Rev. Mod. Phys. **82**, 3045 (2010).
[2] O. Vafek and A. Vishwanath, Annu. Rev. Condens. Matter Phys. **5**, 83 (2014).
[3] X.-G. Wen, Rev. Mod. Phys. **89**, 041004 (2017).
[4] C. L. Kane and E. J. Mele, Phys. Rev. Lett. **95**, 226801 (2005).
[5] B. A. Bernevig, T. L. Hughes, and S.-C. Zhang, Science **314**, 1757 (2006).
[6] M. Z. Hasan and J. E. Moore, Annu. Rev. Condens. Matter Phys. **2**, 55 (2011).
[7] A. Burkov, Nat. Mater. **15**, 1145 (2016).
[8] N. P. Armitage, E. J. Mele, and A. Vishwanath, Rev. Mod. Phys. **90**, 015001 (2018).
[9] C.-K. Chiu, J. C. Y. Teo, A. P. Schnyder, and S. Ryu, Rev. Mod. Phys. **88**, 035005 (2016).
[10] S. Murakami, New J. Phys. **9**, 356 (2007).
[11] S. M. Young, S. Zaheer, J. C. Y. Teo, C. L. Kane, E. J. Mele, and A. M. Rappe, Phys. Rev. Lett. **108**, 140405 (2012).
[12] Z. Liu, B. Zhou, Y. Zhang, Z. Wang, H. Weng, D. Prabhakaran, S.-K. Mo, Z. Shen, Z. Fang, X. Dai *et al.*, Science **343**, 864 (2014).
[13] B. Yan and C. Felser, Annu. Rev. Condens. Matter Phys. **8**, 337 (2017).
[14] Y. Shao, A. Rudenko, J. Hu, Z. Sun, Y. Zhu, S. Moon, A. Millis, S. Yuan, A. Lichtenstein, D. Smirnov *et al.*, Nat. Phys. **16**, 636 (2020).
[15] C. Fang, H. Weng, X. Dai, and Z. Fang, Chin. Phys. B **25**, 117106 (2016).
[16] A. A. Burkov, M. D. Hook, and L. Balents, Phys. Rev. B **84**, 235126 (2011).
[17] M. Z. Hasan, S.-Y. Xu, I. Belopolski, and S.-M. Huang, Annu. Rev. Condens. Matter Phys. **8**, 289 (2017).
[18] D. Vanderbilt, *Berry phases in electronic structure theory: electric polarization, orbital magnetization and topological insulators* (Cambridge University Press, 2018).
[19] E. J. Bergholtz, J. C. Budich, and F. K. Kunst, Rev. Mod. Phys. **93**, 015005 (2021).
[20] Y. Ashida, Z. Gong, and M. Ueda, Adv. Phys. **69**, 249 (2020).
[21] K. Ding, C. Fang, and G. Ma, Nat. Rev. Phys. **4**, 745 (2022).
[22] A. Banerjee, R. Sarkar, S. Dey, and A. Narayan, J. Phys.: Condens. Matter **35**, 333001 (2023).
[23] T. E. Lee, Phys. Rev. Lett. **116**, 133903 (2016).
[24] R. Lin, T. Tai, L. Li, and C. H. Lee, Front. Phys. **18**, 53605 (2023).
[25] F. K. Kunst, E. Edvardsson, J. C. Budich, and E. J. Bergholtz, Phys. Rev. Lett. **121**, 026808 (2018).
[26] L. E. F. Torres, J. Phys. Mater. **3**, 014002 (2020).
[27] D. S. Borgnia, A. J. Kruchkov, and R.-J. Slager, Phys. Rev. Lett. **124**, 056802 (2020).
[28] X. Zhang, T. Zhang, M.-H. Lu, and Y.-F. Chen, Adv. Phys.: X **7**, 2109431 (2022).
[29] S. Yao, F. Song, and Z. Wang, Phys. Rev. Lett. **121**, 136802 (2018).
[30] H. Zhao, X. Qiao, T. Wu, B. Midya, S. Longhi, and L. Feng, Science **365**, 1163 (2019).
[31] A. K. Ghosh and T. Nag, Phys. Rev. B **106**, L140303 (2022).
[32] M.-A. Miri and A. Alu, Science **363**, eaar7709 (2019).
[33] T. Kato, *Perturbation theory for linear operators* (Springer Science & Business Media, 2013), Vol. 132.
[34] K. Kawabata, T. Bessho, and M. Sato, Phys. Rev. Lett. **123**, 066405 (2019).
[35] Z. Yang and J. Hu, Phys. Rev. B **99**, 081102(R) (2019).
[36] J. C. Budich, J. Carlström, F. K. Kunst, and E. J. Bergholtz, Phys. Rev. B **99**, 041406(R) (2019).
[37] L. Zhou and D.-J. Zhang, Entropy **25** (2023).
[38] A. Banerjee and A. Narayan, Phys. Rev. B **102**, 205423 (2020).
[39] T. Oka and H. Aoki, Phys. Rev. B **79**, 081406(R) (2009).
[40] J. Cayssol, B. Dóra, F. Simon, and R. Moessner, Phys. Status Solidi (RRL) **7**, 101 (2013).
[41] Z. Gu, H. A. Fertig, D. P. Arovas, and A. Auerbach, Phys. Rev. Lett. **107**, 216601 (2011).
[42] P. M. Perez-Piskunow, G. Usaj, C. A. Balseiro, and L. E. F. Torres, Phys. Rev. B **89**, 121401(R) (2014).
[43] R. Chen, B. Zhou, and D.-H. Xu, Phys. Rev. B **97**, 155152 (2018).
[44] C.-K. Chan, P. A. Lee, K. S. Burch, J. H. Han, and Y. Ran, Phys. Rev. Lett. **116**, 026805 (2016).
[45] Z. Yan and Z. Wang, Phys. Rev. Lett. **117**, 087402 (2016).
[46] A. Narayan, Phys. Rev. B **94**, 041409(R) (2016).
[47] D. Chowdhury, A. Banerjee, and A. Narayan, Phys. Rev. A **103**, L051101 (2021).
[48] G. Grosso and G. P. Parravicini, *Solid state physics* (Academic press, 2013).
[49] S. Wu, Z. Zhang, K. Watanabe, T. Taniguchi, and E. Y. Andrei, Nat. Mater. **20**, 488 (2021).
[50] N. F. Yuan, H. Isobe, and L. Fu, Nat. Commun. **10**, 5769 (2019).
[51] A. Shtyk, G. Goldstein, and C. Chamon, Phys. Rev. B **95**, 035137 (2017).
[52] D. Guerci, P. Simon, and C. Mora, Phys. Rev. Res. **4**, L012013 (2022).
[53] T. Wang, N. F. Q. Yuan, and L. Fu, Phys. Rev. X **11**, 021024 (2021).
[54] D. O. Oriekhov, V. P. Gusynin, and V. M. Loktev, Phys. Rev. B **103**, 195104 (2021).

[55] A. Kerelsky, L. J. McGilly, D. M. Kennes, L. Xian, M. Yankowitz, S. Chen, K. Watanabe, T. Taniguchi, J. Hone, C. Dean *et al.*, Nature (London) **572**, 95 (2019).
[56] R. S. Markiewicz, B. Singh, C. Lane, and A. Bansil, arXiv:2105.04546.
[57] F. Bonasera, S.-B. Zhang, L. Privitera, and F. M. D. Pellegrino, Phys. Rev. B **106**, 195115 (2022).
[58] N. T. Hung, J. M. Adhidewata, A. R. T. Nugraha, and R. Saito, Phys. Rev. B **105**, 115142 (2022).
[59] Y.-M. Hu, H.-Y. Wang, Z. Wang, and F. Song, arXiv:2210.13491.
[60] H. Wang, J. Ruan, and H. Zhang, Phys. Rev. B **99**, 075130 (2019).
[61] T.-D. Lee and C.-N. Yang, Phys. Rev. **87**, 410 (1952).
[62] M. Bukov, L. D'Alessio, and A. Polkovnikov, Adv. Phys. **64**, 139 (2015).
[63] M. Holthaus, J. Phys. B: At. Mol. Opt. Phys. **49**, 013001 (2016).
[64] T. Oka and S. Kitamura, Annu. Rev. Condens. Matter Phys. **10**, 387 (2019).
[65] M. S. Rudner and N. H. Lindner, Nat. Rev. Phys. **2**, 229 (2020).
[66] M. S. Rudner and N. H. Lindner, arXiv:2003.08252.
[67] F. Harper, R. Roy, M. S. Rudner, and S. Sondhi, Annu. Rev. Condens. Matter Phys. **11**, 345 (2020).
[68] A. Sen, D. Sen, and K. Sengupta, J. Phys.: Condens. Matter **33**, 443003 (2021).
[69] M. Rodriguez-Vega, M. G. Vergniory, and G. A. Fiete, Phys. Today **75**(5), 42 (2022).
[70] T. Mori, Annu. Rev. Condens. Matter Phys. **14**, 35 (2023).
[71] S. Rahav, I. Gilary, and S. Fishman, Phys. Rev. A **68**, 013820 (2003).
[72] K. Kawabata, K. Shiozaki, M. Ueda, and M. Sato, Phys. Rev. X **9**, 041015 (2019).
[73] P. He and Z.-H. Huang, Phys. Rev. A **102**, 062201 (2020).
[74] H. Wu and J.-H. An, Phys. Rev. B **102**, 041119 (2020).
[75] D. C. Brody, J. Phys. A: Math. Theor. **47**, 035305 (2014).
[76] Y. Chen and H. Zhai, Phys. Rev. B **98**, 245130 (2018).
[77] A. O. Sboychakov, K. I. Kugel, and A. Bianconi, Condensed Matter **7**, 50 (2022).
[78] B.-Y. Wen, J.-Y. Wang, T.-L. Shen, Z.-W. Zhu, P.-C. Guan, J.-S. Lin, W. Peng, W.-W. Cai, H. Jin, Q.-C. Xu *et al.*, Light Sci. Appl. **11**, 235 (2022).
[79] X. Han, A. P. Schnyder, and X. Wu, Phys. Rev. B **107**, 184504 (2023).
[80] Y. Li and C. Argyropoulos, IEEE Trans. Antennas Propag. **64**, 14 (2021).
[81] A. Chandrasekaran and J. J. Betouras, Phys. Rev. B **105**, 075144 (2022).
[82] L. Li, S. Ren, W. Qin, S. Zhang, X. Wan, Y. Jia, P. Cui, and Z. Zhang, Phys. Rev. B **102**, 035150 (2020).
[83] Y. Plotnik, M. C. Rechtsman, D. Song, M. Heinrich, J. M. Zeuner, S. Nolte, N. Malkova, J. Xu, A. Szameit, Z. Chen *et al.*, Nat. Mater. **13**, 57 (2014).
[84] Q. Zhong, J. Ren, M. Khajavikhan, D. Christodoulides, S. Ozdemir, and R. El-Ganainy, Phys. Rev. Lett. **122**, 153902 (2019).
[85] S. V. Boriskina, H. Ghasemi, and G. Chen, Mater. Today **16**, 375 (2013).
[86] H. Zhou, C. Peng, Y. Yoon, C. W. Hsu, K. A. Nelson, L. Fu, J. D. Joannopoulos, M. Soljačić, and B. Zhen, Science **359**, 1009 (2018).
[87] A. Cerjan, S. Huang, M. Wang, K. P. Chen, Y. Chong, and M. C. Rechtsman, Nat. Photon. **13**, 623 (2019).
[88] E. J. Bergholtz and J. C. Budich, Phys. Rev. Res. **1**, 012003 (2019).
[89] X.-X. Zhang and M. Franz, Phys. Rev. Lett. **124**, 046401 (2020).
[90] C. H. Lee, S. Imhof, C. Berger, F. Bayer, J. Brehm, L. W. Molenkamp, T. Kiessling, and R. Thomale, Commun. Phys. **1**, 39 (2018).
[91] J. Dong, V. Juričić, and B. Roy, Phys. Rev. Res. **3**, 023056 (2021).
[92] L. Li, C. H. Lee, and J. Gong, Phys. Rev. Lett. **124**, 250402 (2020).
[93] G. Jotzu, M. Messer, R. Desbuquois, M. Lebrat, T. Uehlinger, D. Greif, and T. Esslinger, Nature (London) **515**, 237 (2014).
[94] H. Shen and L. Fu, Phys. Rev. Lett. **121**, 026403 (2018).
[95] L. Fan, K. Wang, H. Wang, A. Dutt, and S. Fan, Sci. Adv. **9**, eadi4956 (2023).